POLARIMETRIC DETECTION OF TARGETS IN INHOMOGENEOUS CLUTTER

Martin Hurtado and Arye Nehorai

Department of Electrical and Systems Engineering
Washington University in St. Louis
One Brookings Drive
St. Louis, MO 63130
{mhurta3, nehorai}@ese.wustl.edu

ABSTRACT

Polarization diversity in radar is useful to detect targets, particularly when Doppler discrimination is not possible. We introduce a new polarimetric radar model that includes the realistic dependence of the clutter reflections on the transmitted signal. We then develop a statistical polarimetric detection test, robust to heavy inhomogeneous clutter. We prove that the detector's false-alarm rate is invariant to the space and time variabilities of the clutter; hence, it has the constant false-alarm (CFAR) property, while still maintaining a good probability of detection. We demonstrate the improved performance of the proposed detector in comparison with existing detectors using numerical examples and real data.

1. INTRODUCTION

The detection of static or slowly moving targets in heavy cluttered environments is considered a challenging problem, mainly because it is not possible to discriminate the target from the clutter using the Doppler effect. Polarization diversity provides additional information that enhances the detection of targets, particularly under the conditions described above.

Earlier work in the field of polarimetric detection has addressed the design of detectors under the assumption that training data is available [1]-[3]. The performance of these detectors can be severely degraded in the presence of inhomogeneous and non-stationary clutter. To overcome this problem, the application of compound-Gaussian distributions for modeling the global behavior of nonhomogeneous clutter has been proposed. However, the use of non-Gaussian models increases the difficulty of developing efficient detection algorithms. For instance, the detection statistic derived from the scheme presented in [4] has a closed-form expression only for the special case of two polarimetric channels, and the detector proposed in [5] does not support the constant false-alarm rate (CFAR) property with respect to the clutter covariance.

In this paper, we develop a polarimetric detector whose decision-making capability is based on the data collected only from the range cell under test, without resorting to secondary data or prior knowledge of the target and clutter. In order to derive the detector, we first introduce a new polarimetric radar model that states the dependence of the clutter reflections on the transmitted signal. We prove that it is robust against inhomogeneous and non-stationary clutter; i.e. the detector's false-alarm rate is insensitive to space and time variations of the clutter, while still maintaining a good probability of detection. Moreover, this test is CFAR. In that sense, this detector resembles that of [6]; however, our work is distinctive in several ways: *(i)* The detector in [6] is developed under the assumption that the target is present only in one of the multiple scans of the radar dwell; thus, it will not detect a static target. Our method is specifically aimed at detecting static or slow targets. *(ii)* Our detector has been extended to consider any arbitrary transmit polarization. *(iii)* Our detector can also be applied to advanced polarimetric receivers, such as tripoles and vector-sensor antennas, in addition to conventional vertical and horizontal (or left and right circular) polarized arrays of antennas. *(iv)* Our detector is tested with real radar data. An additional advantage of our detection algorithm is that it is computationally less intense because it does not require processing of training data.

2. POLARIMETRIC RADAR MODEL

We consider a mono-static radar capable of transmitting waveforms with any arbitrary polarization on a pulse-by-pulse basis. In addition, we assume that the radar system illuminates a point target. The recorded data from the range cell

This work was supported by the Department of Defense under the Air Force Office of Scientific Research MURI Grant FA9550-05-0443, AFOSR Grant FA 9550-05-1-0018 and DARPA under NRL Grant N00173-06-1G006.

under test consist not only of the target echoes but also of the undesired reflections from the target environment (clutter).

2.1. Polarimetric Data

The output of a diversely polarized array of Q sensors receiving the echoes from the cell under test can be expressed as

$$\boldsymbol{y}(t) = B\left(S^{\mathrm{t}} + S^{\mathrm{c}}\right)\boldsymbol{\xi}(t) + \boldsymbol{e}(t),\ t = 1, \ldots, N, \quad (1)$$

where

- The $Q \times 1$ vector $\boldsymbol{y}(t)$ is the complex envelope of the measurements.
- The $Q \times 2$ matrix B is the response of the diversely polarized sensor array. If the receiver array is a vector sensor [7], the array response is given by

$$B = \begin{bmatrix} -\sin\phi & -\cos\phi\sin\psi \\ \cos\phi & -\sin\phi\sin\psi \\ 0 & \cos\psi \\ -\cos\phi\sin\psi & \sin\phi \\ -\sin\phi\sin\psi & -\cos\phi \\ \cos\psi & 0 \end{bmatrix}, \quad (2)$$

  where ϕ and ψ are the azimuth and elevation angles of the cell under test, respectively. For a conventional polarized radar measuring the horizontal and vertical components of the electric field and assuming these two sensors are orthogonal to the direction that points toward the cell under test, the array response matrix is $B = I_2$, where I_2 is the 2×2 identity matrix.

- The complex scattering matrix S represents the polarization change of the transmitted signal upon its reflection on the target or clutter:

$$S = \begin{bmatrix} s_{11} & s_{12} \\ s_{21} & s_{22} \end{bmatrix}, \quad (3)$$

  where the variables s_{11} and s_{22} are co-polar scattering coefficients and s_{12} and s_{21} are cross-polar coefficients. For the mono-static radar case, $s_{12} = s_{21}$. The superscripts $^{\mathrm{t}}$ and $^{\mathrm{c}}$ refer to the target and clutter.

- The vector $\boldsymbol{\xi}(t)$ is the narrowband transmitted polarized signal which can be represented by

$$\boldsymbol{\xi}(t) = \begin{bmatrix} \xi_1 \\ \xi_2 \end{bmatrix} s(t) = \begin{bmatrix} \cos\alpha & \sin\alpha \\ -\sin\alpha & \cos\alpha \end{bmatrix} \begin{bmatrix} \cos\beta \\ j\sin\beta \end{bmatrix} s(t), \quad (4)$$

  where ξ_1 and ξ_2 are the signal components on the polarization basis of the transmitter, α and β are the orientation and ellipticity angles, respectively, and $s(t)$ is the complex envelope of the transmitted signal.

- The vector $\boldsymbol{e}(t)$ represents the thermal noise.

Equation (1) can be written as

$$\boldsymbol{y}(t) = s(t)B\bar{\xi}\left(\boldsymbol{\mu} + \boldsymbol{x}\right) + \boldsymbol{e}(t), \quad (5)$$

where the scattering coefficient vectors of the target and clutter are $\boldsymbol{\mu} = [s^{\mathrm{t}}_{\mathrm{hh}}, s^{\mathrm{t}}_{\mathrm{vv}}, s^{\mathrm{t}}_{\mathrm{hv}}]^T$ and $\boldsymbol{x} = [s^{\mathrm{c}}_{\mathrm{hh}}, s^{\mathrm{c}}_{\mathrm{vv}}, s^{\mathrm{c}}_{\mathrm{hv}}]^T$, respectively, which have dimension $P = 3$. The polarization matrix $\bar{\xi}$ is

$$\bar{\xi} = \begin{bmatrix} \xi_1 & 0 & \xi_2 \\ 0 & \xi_2 & \xi_1 \end{bmatrix}. \quad (6)$$

The time samples can be stacked in one vector of dimension $NQ \times 1$:

$$\boldsymbol{y} = \left(\boldsymbol{s} \otimes B\bar{\xi}\right)\left(\boldsymbol{\mu} + \boldsymbol{x}\right) + \boldsymbol{e}, \quad (7)$$

where $\boldsymbol{s} = [s(1), \ldots, s(N)]^T$ and $\otimes$ is the Kronecker product. Piling together the data corresponding to pulses of different polarization yields

$$\boldsymbol{y} = A\boldsymbol{\mu} + A\boldsymbol{x} + \boldsymbol{e}, \quad (8)$$

where A is a $M \times P$ ($M = KNQ$) complex matrix that represents the system response:

$$A = \begin{bmatrix} \boldsymbol{s} \otimes B\bar{\xi}_1 \\ \vdots \\ \boldsymbol{s} \otimes B\bar{\xi}_K \end{bmatrix}, \quad (9)$$

and $\bar{\xi}_k$ is the polarization matrix of each diversely polarized pulse ($k = 1, \ldots, K$).

2.2. Statistical Model

We assume that the target is a small man-made object; hence, $\boldsymbol{\mu}$ is a deterministic vector. On the other hand, the clutter in the range cell under test can be considered as a large collection of point scatterers producing incoherent reflections of the radar signal. Then, $\boldsymbol{x}$ is a zero-mean complex Gaussian random vector with covariance matrix Σ. The noise $\boldsymbol{e}$ is a zero-mean complex Gaussian random vector with covariance matrix σI_M, where I_M is the $M \times M$ identity matrix. In addition, we assume that the clutter reflections and the thermal noise are statistically independent.

The radar dwell consists of a series of pulses that can be seen as "snapshots" of the range cell under test. If the pulse duration is short with respect to the dynamic of the target and its environment, it is reasonable to assume that their scattering coefficients are constant during each pulse. However, from pulse to pulse, we consider the clutter scattering coefficients as independent realizations of the same random process. Then, the distribution of each snapshot is

$$\boldsymbol{y}_d \sim \mathcal{CN}(A\boldsymbol{\mu}, A\Sigma A^H + \sigma I_M), \quad d = 1, \ldots, D, \quad (10)$$

where D is the total number of snapshots or pulses in the radar dwell and ^{H} denotes the conjugate transpose operator.

2.3. Known and Unknown Model Parameters

We assume the system response matrix A is known, since we consider that the receiver antenna array has been calibrated. In addition, we assume that the power of the thermal noise σ is known, because it can be easily estimated from the recorded data when no signal has been transmitted. However, we suppose that we have no prior knowledge about the target and the clutter, nor do we count on a secondary data set for estimating the statistical properties of the clutter. Hence, the vector $\boldsymbol{\mu}$ and the matrix Σ are the unknown parameters of the statistical data model (10).

3. DETECTION TEST

We aim to decide whether a target is present or not in the range cell under test, based on the recorded data. Then, the decision problem consists of choosing between two possible hypotheses: the null hypothesis $\mathcal{H}_0$ (target-free hypothesis) or the alternative hypothesis $\mathcal{H}_1$ (target-present hypothesis)

$$\begin{cases} \mathcal{H}_0: & \boldsymbol{\mu} = 0,\ \Sigma \\ \mathcal{H}_1: & \boldsymbol{\mu} \neq 0,\ \Sigma \end{cases} \tag{11}$$

where the matrix Σ is considered as a nuisance parameter. Next, we derive the generalized likelihood ratio (GLR) test [8] and study its performance. We omit derivation details in this paper due to space limitation; refer to [9] for an extended version of this paper.

3.1. GLR Test

The GLR test decides $\mathcal{H}_1$ if

$$L_{\mathrm{GLR}} = \frac{f_1(\boldsymbol{y}_1, \ldots, \boldsymbol{y}_D; \hat{\boldsymbol{\mu}}_1, \hat{\Sigma}_1)}{f_0(\boldsymbol{y}_1, \ldots, \boldsymbol{y}_D; \hat{\Sigma}_0)} > \gamma, \tag{12}$$

where f_0 and f_1 are the likelihood functions under $\mathcal{H}_0$ and $\mathcal{H}_1$, $\hat{\Sigma}_0$ and $\hat{\Sigma}_1$ are the maximum likelihood estimates (MLE) of Σ under $\mathcal{H}_0$ and $\mathcal{H}_1$, $\hat{\boldsymbol{\mu}}_1$ is the MLE of $\boldsymbol{\mu}$ under $\mathcal{H}_1$, and γ is the detection threshold. For simplicity of notation we will omit references to the data in the arguments of the functions f_0 and f_1 in the rest of the paper.

We start the derivation of the GLR test by determining the likelihood functions and MLEs of the unknown parameters. Under hypothesis $\mathcal{H}_0$, it is assumed that $\boldsymbol{\mu} = 0$; then

$$\ln f_0(\Sigma) = -D\left[M \ln \pi + \ln |C| + \mathrm{tr}(C^{-1} S_0)\right], \tag{13}$$

where $C = A\Sigma A^H + \sigma I_M$ is the theoretical covariance matrix of the data, defined in (10), and S_0 is the sample covariance matrix

$$S_0 = \frac{1}{D} \sum_{d=1}^{D} \boldsymbol{y}_d \boldsymbol{y}_d^H. \tag{14}$$

The MLE of Σ is

$$\hat{\Sigma}_0 = A^+ S_0 A^{+H} - \sigma (A^H A)^{-1}, \tag{15}$$

where $A^+ = (A^H A)^{-1} A^H$ is the generalized matrix inverse. Under hypothesis $\mathcal{H}_1$, the likelihood function is

$$\ln f_1(\boldsymbol{\mu}, \Sigma) = -D\left[M \ln \pi + \ln |C| + \mathrm{tr}(C^{-1} \tilde{C}_1)\right], \tag{16}$$

where

$$\tilde{C}_1 = \frac{1}{D} \sum_{d=1}^{D} (\boldsymbol{y}_d - A\boldsymbol{\mu})(\boldsymbol{y}_d - A\boldsymbol{\mu})^H. \tag{17}$$

The MLE of the unknown parameters are

$$\hat{\boldsymbol{\mu}}_1 = A^+ \bar{\boldsymbol{y}}, \tag{18}$$

$$\hat{\Sigma}_1 = A^+ S_1 A^{+H} - \sigma (A^H A)^{-1}, \tag{19}$$

where $\bar{\boldsymbol{y}}$ is the sample mean vector

$$\bar{\boldsymbol{y}} = \frac{1}{D} \sum_{d=1}^{D} \boldsymbol{y}_d, \tag{20}$$

and S_1 is the sample covariance matrix

$$S_1 = \frac{1}{D} \sum_{d=1}^{D} (\boldsymbol{y}_d - \bar{\boldsymbol{y}})(\boldsymbol{y}_d - \bar{\boldsymbol{y}})^H. \tag{21}$$

Then, substituting the MLEs and likelihood functions in (12), and after some mathematical simplifications, the GLR test can be written as

$$L_{\mathrm{GLR}} = \left[1 + \bar{\boldsymbol{y}}^H A \left(A^H S_1 A\right)^{-1} A^H \bar{\boldsymbol{y}}\right]^D. \tag{22}$$

Since (22) is a monotonically increasing function of the second term inside the brackets, an equivalent detection test statistic can be defined as

$$T_{\mathrm{GLR}} = \bar{\boldsymbol{y}}^H A \left(A^H S_1 A\right)^{-1} A^H \bar{\boldsymbol{y}}. \tag{23}$$

3.2. Detection Performance

Applying Corollary 5.2.1 from [10], it is straightforward to verify that the detection statistic (23) is distributed as follows

$$T_{\mathrm{GLR}} \frac{D-P}{P} \sim \begin{cases} \mathcal{F}_{2P,2(D-P)} & \text{under } \mathcal{H}_0 \\ \mathcal{F}'_{2P,2(D-P)}(\lambda) & \text{under } \mathcal{H}_1 \end{cases} \tag{24}$$

where $\mathcal{F}_{\nu_1,\nu_2}$ denotes an F distribution with ν_1 and ν_2 degrees of freedom, and $\mathcal{F}'_{\nu_1,\nu_2}(\lambda)$ denotes a non-central F distribution with ν_1 and ν_2 degrees of freedom and non-centrality parameter λ. The non-centrality parameter is given by

$$\lambda = 2D\boldsymbol{\mu}^H \left[\Sigma + \sigma \left(A^H A\right)^{-1}\right]^{-1} \boldsymbol{\mu}. \tag{25}$$

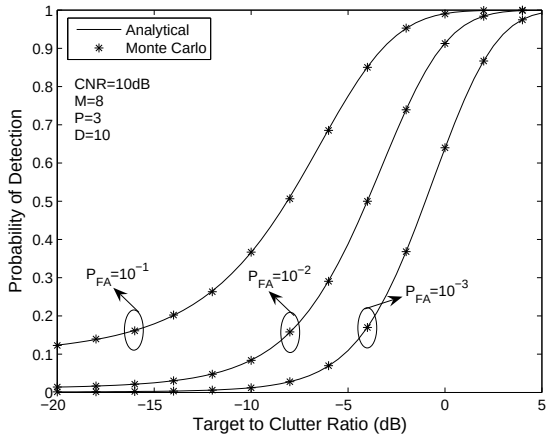

Figure 1: Detection performance of the GLR test statistic T_{GLR} as a function of the target-to-clutter ratio, for different values of P_{FA}.

Thus, the detection performance becomes

$$\begin{aligned} P_{\mathrm{FA}} &= Q_{\mathcal{F}_{2P,2(D-P)}}(\gamma) \\ P_{\mathrm{D}} &= Q_{\mathcal{F}'_{2P,2(D-P)}(\lambda)}(\gamma), \end{aligned} \tag{26}$$

where P_{D} is the probability of detection, P_{FA} is the probability of false alarm, Q is the right-tail probability function [8, Chap. 2] and γ is the detection threshold for the required probability of false alarm. In particular, note that the expression for P_{FA} does not depend on the covariance of clutter and thermal noise, nor on the transmitted signal; hence, equation (23) is a CFAR test.

We validated the analytical performance of the developed test by computer simulations. We performed Monte Carlo simulations based on $100/P_{\mathrm{FA}}$ independent trails. Figure 1 shows curves of P_{D} as a function of target-to-clutter ratio (TCR) for different values of P_{FA} and a clutter-to-noise ratio (CNR) of 10dB. The definitions of TCR and CNR are given in the Appendix. The results depicted in the figure consist of the average of 100 different cases. For each case, the entries of $\boldsymbol{\mu}$, Σ, and A are independent realization of a random variable with distribution $\mathcal{CN}(0,1)$; then those vectors and matrices are scaled to fulfill the required TCR and CNR.

3.3. Detector Performance in Inhomogeneous Clutter

A significant characteristic of the detector presented in this paper is that the test statistic (23) is computed using only data from the cell under test. No assumption is required about the range homogeneity of the clutter. Thus, the detector is robust against spatially fluctuating clutter.

To support this assertion, the P_{FA} is computed using $5 \cdot 10^5$ runs of Monte Carlo simulations in the presence of inhomogeneous clutter. The clutter echoes are assumed to follow a compound-Gaussian distribution with covariance matrix $\tau\Sigma$. The texture τ has a generalized Gamma probability density function [4]:

$$p(\tau) = \frac{1}{\Gamma(\nu)} \left(\frac{\nu}{\delta}\right)^{\nu} \tau^{\nu-1} \exp\left(-\frac{\nu}{\delta}\tau\right), \tag{27}$$

where ν is the order parameter and δ is the average power. Note that $\nu = \infty$ corresponds to clutter echoes with Gaussian distribution, but when ν decreases, they deviate from Gaussian. Additional information about the simulation setup is as follows. The transmitted signals are rectangular pulses, which are transmitted in a sequence of alternating vertical (V) and horizontal (H) polarization ($K = 2$). The radar dwell consists of 10 repetitions of this polarimetric sequence ($D = 10$). On the receiver side, samples of the V and H electric field are recorded ($Q = 2$) at a rate of one sample per pulse ($N = 1$). Since the simulations are intended to compute the P_{FA}, no target is considered. The average power of the texture is $\delta = 50$ and the speckle component of the covariance is $\Sigma = I_3$.

For comparison purposes, we also compute the performance of other detectors that use secondary data:

- Polarization-space-time GLR (PST-GLR): This detector was derived under the assumption of homogeneous Gaussian clutter [1].
- Texture free GLR (TF-GLR): This detector was formulated assuming that the clutter follows a compound Gaussian distribution [4].
- Hybrid U test: This detector was developed for a single polarimetric channel assuming that the clutter follows a Weibull distribution [11].

In Fig. 2, the P_{FA} of our detection test T_{GLR}, as well as of the PST-GLR, TF-GLR, and Hybrid U tests, is plotted as a function of the order parameter of the clutter texture distribution. For the latter three tests, we consider 80 adjacent range cells for generating the secondary data. We observe that the performance of our detector T_{GLR} and the TF-GLR test remains constant at the designed false-alarm rate. However, there is a discrepancy between the design and the actual clutter that increases the probability of false alarm for the PST-GLR test as the clutter process departs from being Gaussian. The Hybrid U test behaves similar to the PST-GLR; but it has larger P_{FA} due to the mismatch between the model used to generate the clutter data and the one assumed by the algorithm.

3.4. Detector Performance Using Real Data

To evaluate the performance of the polarimetric detectors in a real application situation, we use data collected at the

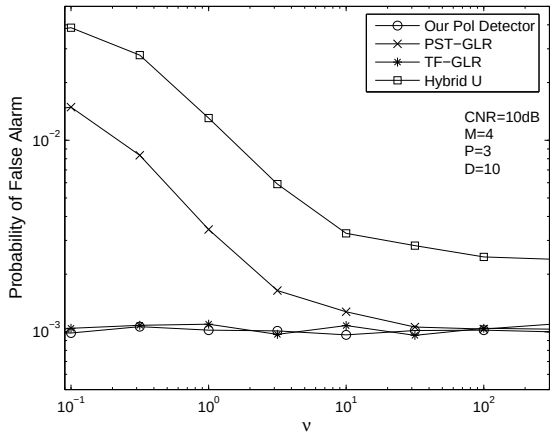

Figure 2: Probability of false alarm as a function of the order parameter ν of the clutter texture distribution.

Osborne Head Gunnery Range (OHGR), Dartmouth, Nova Scotia, Canada, with the McMaster University IPIX radar [12]. Specifically, we use the data recorded on November 11, 1993. Fig. 3 shows the magnitude of the echoes from a small target in inhomogeneous sea clutter for the four polarimetric channels: HH, VH, VV, and HV.

Fig. 4 shows detection maps for the T_{GLR}, PST-GLR, TF-GLR, and Hybrid U tests. The detection threshold is again set for $P_{\mathrm{FA}} = 10^{-3}$, and other parameters are also as in the former subsection. For the latter three tests, a guard region of two range cells on either side of the cell under test is used to avoid the leakage of the target energy into the secondary data. We observe that our detection test finds the true position of the target with only a few false detections despite the strong clutter echoes, which can be appreciated from Fig. 3. On the other hand, the PST-GLR has high false-alarm rate due to the presence of inhomogeneous clutter, as was predicted in the previous subsection. The Hybrid U and TF-GLR tests reduce the false-alarm rate with respect to the PST-GLR test; however, it still remains considerably high.

One possible way of summarizing the performance of these detection tests in relation to real data is to plot the empirical receiver operating characteristic (ROC) curves. The empirical ROC is obtained by dividing the detection map in two regions. One region corresponds to the range where the target is located and the other region corresponds to the range where there is only clutter. For different values of the detection threshold γ, the empirical P_{D} and P_{FA} are computed by counting the pixels on each respective region. Fig. 5 shows that the empirical ROC curve of the T_{GLR} test is on the top, outperforming the other algorithms.

We acknowledge that comparing the Hybrid U and TF-GLR tests with the other two is not strictly fair, since these

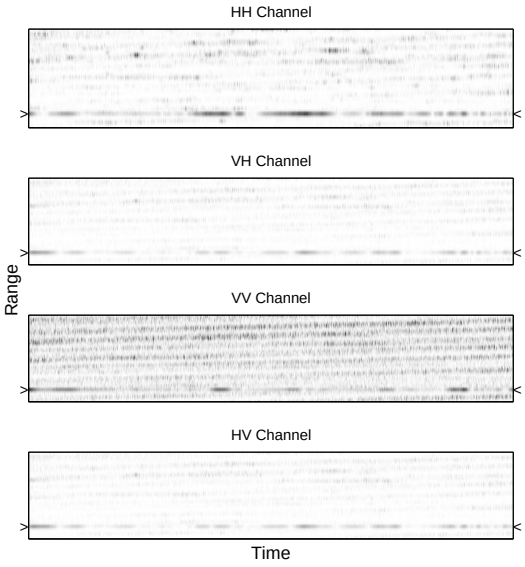

Figure 3: Magnitude in range and time domain of the IPIX radar dataset *stare1*, collected on November 11, 1993. The target location is indicated by the markers "$>$" and "$<$".

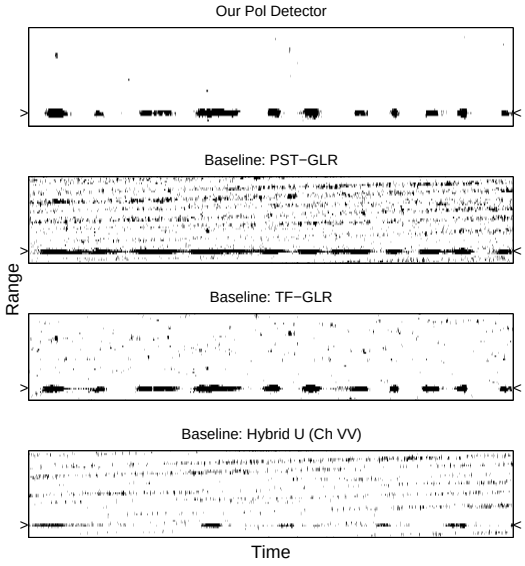

Figure 4: Detection map in range and time domain for the IPIX radar dataset *stare1*, collected on November 11, 1993. Black pixels indicate that the detection statistic is larger than the threshold. The target location is indicated by the markers "$>$" and "$<$".

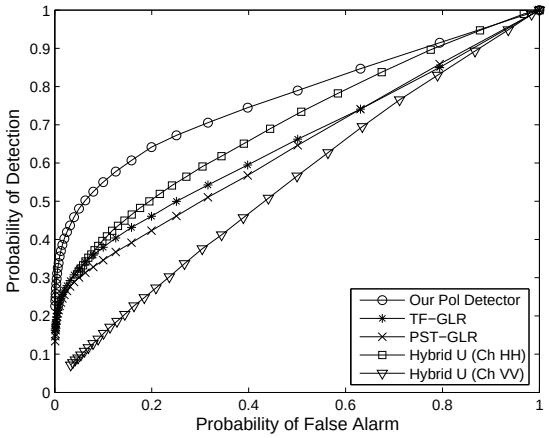

Figure 5: Empirical receiver operating characteristic (ROC) curves.

tests were developed for one and two polarimetric channels, respectively. (We have used HH and VV for the previous results of the TF-GLR test.) Our goal is not to extend these algorithms but to show that detection tests using secondary data may have larger false false-alarm than their designed value, in the case of inhomogeneous clutter.

4. CONCLUSIONS

In this paper, we addressed the problem of detecting small and slowly moving targets in heavy inhomogeneous clutter by exploiting polarization diversity. We first introduced a data model that states the dependency of the clutter reflections on the transmitted signal. Then, we developed a new polarimetric detector that is robust against space and time variations of the clutter. The proposed detector decides the presence of a target based only on the data recorded from the cell under test, without requiring secondary data or prior knowledge about the clutter. We studied its performance and demonstrated that it supports the CFAR property. We tested this detector with synthetic and real data, showing significant performance improvement with respect to other detectors. An additional advantage of our detection algorithm is that it is computationally less intense because it does not require recording and processing of training data.

5. APPENDIX

The target-to-clutter ratio and clutter-to-noise ratio are

$$\mathrm{TCR} = \frac{||\boldsymbol{\mu}||^2}{\mathrm{tr}(\Sigma)}, \quad \mathrm{CNR} = \frac{\mathrm{tr}(\Sigma)}{\sigma},$$

where $||\cdot||$ is the norm of the vector.

6. REFERENCES

[1] H. Park, J. Li, and H. Wang, "Polarization-space-time domain generalized likelihood ratio detection of radar targets," *Signal Processing,* Vol. 41, pp. 153-164, Jan. 1995.

[2] D. Pastina, P. Lombardo, and T. Bucciarelli, "Adaptive polarimetric target detection with coherent radar. Part I: Detection against Gaussian background," *IEEE Trans. Aerosp. Electr. Syst.*, Vol. 37, pp. 1194-1206, Oct. 2001.

[3] A. De Maio and G. Ricci, "A polarimetric adaptive matched filter," *Signal Processing,* Vol. 81, pp. 2583-2589, Dec. 2001.

[4] P. Lombardo, D. Pastina, and T. Bucciarelli, "Adaptive polarimetric target detection with coherent radar. Part II: Detection against non-Gaussian background," *IEEE Trans. Aerosp. Electr. Syst.,* Vol. 37, pp. 1207-1220, Oct. 2001.

[5] A. De Maio and G. Alfano, "Polarimetric adaptive detection in non-Gaussian noise," *Signal Processing,* Vol. 83, pp. 297-306, Feb. 2003.

[6] R. Brown and H. Wang, "An adaptive multiscan processor for polarimetric radar," *IEEE National Radar Conference,* 29-31 Mar. 1994, pp. 95-100.

[7] A. Nehorai and E. Paldi, "Vector-sensor array processing for electromagnetic source localization," *IEEE Trans. Signal Process.*, Vol. 42, pp. 376-398, Feb. 1994.

[8] S. M. Kay, *Fundamentals of Statistical Signal Processing: Detection Theory*, Englewood Cliffs, NJ: Prentice Hall, 1993.

[9] M. Hurtado and A. Nehorai, "Polarimetric detection of targets in heavy inhomogeneous clutter," submitted to *IEEE Trans. Signal Process.*

[10] T. W. Anderson, *An Introduction to Multivariate Statistical Analysis*, 3rd Ed., Hoboken, NJ: John Wiley & Sons, 2003.

[11] B. Dawber and J. Branson,"Use of site specific radar modelling to improve CFAR performance in the littoral,"*IEEE Int. Conf. Radar,* pp. 161-166, 9-12 May 2005.

[12] S. Haykin, C. Krasnor, T. J. Nohara, B. W. Currie, and D. Hamburger, "A coherent dual-polarized radar for studying the ocean environment," *IEEE Trans. Geosci. Remote Sensing,* Vol. 29, pp. 189-191, Jan. 1991.